Time-varying characteristics of saturated hydraulic conductivity in grassed swales based on the ensemble Kalman filter algorithm

A case study of two long-running swales in Netherlands

Yang, Feikai; Fu, Dafang; Zevenbergen, Chris; Boogaard, Floris C.; Singh, Rajendra Prasad

DOI
10.1016/j.jenvman.2023.119760

Publication date
2023

Document Version
Final published version

Published in
Journal of Environmental Management

Citation (APA)
Yang, F., Fu, D., Zevenbergen, C., Boogaard, F. C., & Singh, R. P. (2023). Time-varying characteristics of saturated hydraulic conductivity in grassed swales based on the ensemble Kalman filter algorithm: A case study of two long-running swales in Netherlands. *Journal of Environmental Management*, *351*, Article 119760. https://doi.org/10.1016/j.jenvman.2023.119760

Journal of Environmental Management 351 (2024) 119760

Contents lists available at ScienceDirect

Journal of Environmental Management

journal homepage: www.elsevier.com/locate/jenvman

Research article

Time-varying characteristics of saturated hydraulic conductivity in grassed swales based on the ensemble Kalman filter algorithm —A case study of two long-running swales in Netherlands

Feikai Yang [a,b,c,d], Dafang Fu [a,b], Chris Zevenbergen [c,d], Floris C. Boogaard [e,f], Rajendra Prasad Singh [a,b,*]

[a] School of Civil Engineering, Southeast University, Nanjing 210096, China
[b] Southeast University-Monash University Joint Research Centre for Future Cities, Nanjing 210096, China
[c] IHE-Delft Institute for Water Education, P.O. Box 3015, 2611DA Delft, the Netherlands
[d] Department of Civil Engineering, Delft University of Technology (TU Delft), Gebouw 23, Stevinweg 1, 2628CN Delft, the Netherlands
[e] Research Centre for Built Environment NoorderRuimte, Hanze University of Applied Sciences, 9747 AS Groningen, the Netherlands
[f] Deltares, Daltonlaan 600, 3584 BK Utrecht, the Netherlands

ARTICLE INFO

Handling Editor: Jason Michael Evans

Keywords:
Grassed swales
Saturated hydraulic conductivity
Ensemble Kalman filter
Multivariate nonlinear regression
Nature based solution

ABSTRACT

Saturated hydraulic conductivity (K_s) of the filler layer in grassed swales are varying in the changing environment. In most of the hydrological models, K_s is assumed as constant or decrease with a clogging factor. However, the K_s measured on site cannot be the input of the hydrological model directly. Therefore, in this study, an Ensemble Kalman Filter (EnKF) based approach was carried out to estimate the K_s of the whole systems in two monitored grassed swales at Enschede and Utrecht, the Netherlands. The relationship between K_s and possible influencing factors (antecedent dry period, temperature, rainfall, rainfall duration, total rainfall and seasonal factors) were studied and a Multivariate nonlinear function was established to optimize the hydrological model. The results revealed that the EnKF method was satisfying in the K_s estimation, which showed a notable decrease after long-term operation, but revealed a recovery in summer and winter. After the addition of Multivariate nonlinear function of the K_s into hydrological model, 63.8% of the predicted results were optimized among the validation events, and compared with constant K_s. A sensitivity analysis revealed that the effect of each influencing factors on the K_s varies depending on the type of grassed swale. However, these findings require further investigation and data support.

1. Introduction

Global warming has led to an increase in the frequency and severity of extreme weather events, such as floods and droughts (Wu et al., 2022; Corner, 2022). In response to these challenges, numerous initiatives have been proposed and implemented. Notably, best management practices (BMPs) have emerged as a significant approach in the United States (Fletcher et al., 2015), sustainable urban drainage systems (SUDSs) in UK (Ellis et al., 2022), water sensitive urban design in Australia (Xiufeng et al., 2019) and sponge cities in China. Grassed swales are the most common BMP facilities and widely employed in the construction of sponge cities due to their excellent water transfer capabilities (Saracoglu and Kazezyilmaz-Alhan, 2023). Their effectiveness in efficiently managing water flow has made them a popular choice within this context. Saturated hydraulic conductivity (K_s) is the most important parameter to characterize the hydrological effect of grassed swales (Tarek et al., 2022). The characteristics of the rainfall events (including intensity, duration and antecedent dry period) and the watersheds (including land cover, surface area, slope and drainage patterns) combinedly determine the formation of runoff into the grassed swale (Shafique et al., 2018). The storage capacity of the grassed swales increases the infiltration and delay the outflow.

Most of the researches on grassed swales and similar facilities in the past 20 years focused only on the initial K_s and its value after a long-term running (Haile et al., 2016; Willard et al., 2017; Kluge et al., 2018). A bioretention system in Blacksburg, USA, exhibited good runoff and

* Corresponding author. School of Civil Engineering, Southeast University, Nanjing 210096, China.
E-mail address: rajupsc@seu.edu.cn (R.P. Singh).

https://doi.org/10.1016/j.jenvman.2023.119760
Received 1 July 2023; Received in revised form 1 December 2023; Accepted 1 December 2023
Available online 12 December 2023

infiltration capacity after 7 years of operation (Willard et al., 2017), while another study of two biofiltration systems which had been operated for 9 and 14 years in Sweden, became entirely blocked (Al-Rubaei et al., 2015). These results were different from other similar case studies. In most of the hydrological models, a long-term monitoring data (rainfall, outflow, etc.) were used to calibrate the value of K_s, but this value was often an average value from a series of rainfall events, and regards as constant in the following model prediction (Brown et al., 2013; Abualfaraj et al., 2018). The wildly used SWMM model assume a 'clogging factor' that is the total volume of treated runoff which completely clog the bottom of the layer is divided by the void volume of the layer and a value of 0 to ignore clogging (Rossman, 2015). Clogging is quite common but not all the facilities would be clogged after a long-term operation (Boogaard, 2022; Kluge et al., 2018; Liu et al., 2018). Young et al. (2018) found that the K_s measured on-site could not be directly used as input parameters for the model because a single point value cannot represent the entire system. All these issues increased the uncertainty in the model predictions. Boogaard (2022) found a way to make the system fully saturated and the rate of decrease in surface level was regarded approximately equal to K_s value, but this approximation method needs to be established in the case of a regular surface, and the use of man-made rainfall makes it impossible to become a long-term plan.

There are many environmental factors that might cause the change in K_s. Soil and grassland types have a significant effect on the peak flow reduction and drainage performance of grassed swales (Saracoglu and Kazezyilmaz-Alhan, 2023). Yousef et al. (1987) noted that dense turf can improve the permeability of soil media. Plant roots are capable to increase the local permeability (Geerling, 2014) and form the upper layer of soil with higher permeability (Renato et al., 2016). The planting density and spatial periodicity of plants determine the structure and hydraulic characteristics of the vegetation layer in the grassed swales (Irvine and Kim, 2019). Evapotranspiration is a critical factor for the long-term water balance process of grassed swales which contributes to the restoration of soil permeability during dry days (Deletic, 2000; Boogaard, 2022). Cold climate also affects soil the infiltration rate. Zaqout and Andradóttir (2021) found that the peak flow reduction in winter was three times lower than that in summer. Whereas, some studies pointing out that due to the preferential flow, the saturated hydraulic conductivity of granular or porous media under frost conditions may be greater than that of unfrozen soil (Stoeckeler and Weitzman, 1960; Lefevre et al., 2009).

The Ensemble Kalman filter method is widely used for the prediction of soil moisture content (Amol and Raaj, 2018; Lou et al., 2022), runoff simulation (Fw et al., 2022; Mazrooei and Sankarasubramanian, 2019; Wang et al., 2018) and assimilation of rainfall, snow and evapotranspiration (Girotto et al., 2020; Su et al., 2019; Wei et al., 2018). Jiang et al. (2019) coupled the EnKF method with HYDRUS-1D software to effectively estimate the parameters of layered and variable saturated soils and predict state variables. Akter (2021) used EnKF to estimate the static parameters (i.e. porosity and permeability) and state variables of the aquifer, and established a calculation model combining state estimation and parameter calibration, which is used for parameter estimation of nonlinear two-dimensional aquifers. Although the EnKF method has been applied for the parameter estimation of hydrological models, however, it is rarely used for the long-term identification of time-varying parameters.

Therefore, the current study aims to develop a method to calculate the saturated hydraulic conductivity (K_s) of the whole grassed swale systems in each rainfall event by coupling the hydrological model with the Ensemble Kalman filter algorithm using long-term monitoring data (rainfall, surface water depth (h_p), outflow (q), etc.). Multivariate nonlinear function between K_s and potential influencing factors (antecedent dry period, temperature, rainfall, rainfall duration, total rainfall, and seasonal factors) was established and a time-varying K_s was used to optimize the hydrological model. A sensitivity analysis was also carried out at the end to discern the differences of impact by influencing factors between various swales.

2. Material and methods

2.1. Study sites

The two target swales are located in the Netherlands. First one in the Enschede city, which is the oldest large scale implemented swale system in Netherlands (exact location, photos and videos can be found on https://www.climatescan.org/projects/211/detail). The swale carries runoff from residential roads and rooftops for more than 20 years. This swale is an approximate rectangular structure, consist of filler layer with improved soil and the drainage layer with coarse aggregate. The specific parameters are shown in Table S1. The monitoring period was from May 1999 to May 2002 and November 2020 to October 2021 and the rainfall, temperature, and surface water level were measured. Another swale is located in the Utrecht city (exact location, photos and videos can be found on https://www.climatescan.org/projects/2523/detail). This swale receives surface runoff from the roads and roundabout nearby and has been in operation for more than ten years. It is a T-shaped structure consist of medium coarse sand in both filler layer and drainage layer. Donkers (2010) and Geerling (2014) monitored and compared the hydrological performance of this swale in 2010 and 2014, respectively. The specific characteristics are shown in Table S2. It was put into operation in April 2009. In this study, the monitoring period was from November 2020 to October 2021 and the rainfall, temperature, inflow rate and outflow rate were measured.

2.2. Hydrological model for grassed swales

A hydrological model was built based on the Darcy's formula and water balance equation, which calculates the filler layer and drainage layer as independent units. It was assumed that the infiltration of the filler layer is a process of uniform saturation. The initial infiltration and the emptying stage after rainfall are both unsaturated processes, characterized by unsaturated hydraulic conductivity using van Genuchten formula (Genuchten and Th, 1980).

$$f = K_s\left(1 + \frac{\Delta P}{Z_f}\right) \tag{1}$$

where, f is the infiltration rate, K_s is the saturated hydraulic conductivity, Z_f is the infiltration length and ΔP is the pressure difference at both end of infiltration unit.

$$K(\theta) = K_s\left(\frac{\theta-\theta_r}{\theta_s-\theta_r}\right)^{\frac{1}{2}}\left[1-\left(1-\left(\frac{\theta-\theta_r}{\theta_s-\theta_r}\right)^{\frac{1}{m}}\right)^{m}\right]^2 \tag{2}$$

where, $K(\theta)$ is the unsaturated hydraulic conductivity, θ is the water content, θ_r is the residual water content, n is the empirical fitting parameters or curve shape parameters and m = 1–1/n (Donkers, 2010).

$$P = V_{in} + V_{out} + V_{over} + V_d + E_T \tag{3}$$

where, P is the rainfall, V_{in} is the infiltration volume, V_{out} is the outflow volume, V_{over} is the overflow volume, V_d is the detention volume and E_T is the evapo-transpiration. Evaporation during rainfall was neglected in this study.

The model was verified by 6 artificial rainfalls in a pilot grassed swale in Kunshan, China.

2.3. Ensemble Kalman filter algorithm for K_s assimilation

The ensemble Kalman filtering is a nonlinear filtering algorithm that combines Monte Carlo and Kalman filtering. It generates an ensemble of parameters and state variables through random methods to predict the

model state. The error covariance matrix is updated through the calculate of ensembles, and the mean of the ensemble represents the optimal estimation of the state. The method contains two parts; prediction and assimilation update. The key process of Ensemble Kalman filter is to establish the state transition equation (prediction equation) and observation equation of the modeled system. The general state transition equation is as follows:

$$\boldsymbol{x}_{i+1} = \boldsymbol{f}(\boldsymbol{x}_i, \boldsymbol{\theta}) + \boldsymbol{\varepsilon}_i, \boldsymbol{\varepsilon}_i \sim N(\boldsymbol{0}, \boldsymbol{Q}_i) \tag{4}$$

where, $\boldsymbol{x}_{i+1}$ is the state variables, $\boldsymbol{f}$ is the hydrological model, $\boldsymbol{\theta}$ is the parameters, $\boldsymbol{\varepsilon}_i$ is the model error which obeys the normal distribution.

The observation equation is as follows:

$$\boldsymbol{y}_{i+1} = \boldsymbol{h}(\boldsymbol{x}_{i+1}, \boldsymbol{\theta}) + \boldsymbol{\delta}_{i+1}, \boldsymbol{\delta}_{i+1} \sim N(\boldsymbol{0}, \boldsymbol{R}_{i+1}) \tag{5}$$

where, $\boldsymbol{y}_{i+1}$ is the observation vector, $\boldsymbol{h}$ is the conversion relationship between the state variables and the observed values refers to the hydrological model in this study, $\boldsymbol{\delta}_{i+1}$ is the observation error which obeys the normal distribution.

The assimilation process of ensemble Kalman filter is as follows:

$$\boldsymbol{x}^k_{i+1|i} = \boldsymbol{f}\left(\boldsymbol{x}^k_{i|i}, \boldsymbol{\theta}\right) + \boldsymbol{\varepsilon}^k_i \tag{6}$$

$$\boldsymbol{x}^k_{i+1|i+1} = \boldsymbol{K}_{i+1}\left(\boldsymbol{y}^k_{i+1} - \boldsymbol{h}\left(\boldsymbol{x}^k_{i+1|i}, \boldsymbol{\theta}\right)\right) \tag{7}$$

$$\boldsymbol{y}^k_{i+1} = \boldsymbol{y}_{i+1} + \boldsymbol{\delta}^k_{i+1} \tag{8}$$

where, $\boldsymbol{x}^k_{i+1|i}$ is the predicted value of kth ensemble at time $i+1$, $\boldsymbol{x}^k_{i|i}$ is the update value of the kth ensemble at time i, $\boldsymbol{\varepsilon}^k_i$ is the white noise of the kth ensemble, $\boldsymbol{y}^k_{i+1}$ is the observation of the kth ensemble, $\boldsymbol{\delta}^k_{i+1}$ is the observation error of the kth ensemble, $\boldsymbol{K}_{i+1}$ is the Kalman gain, which represents the weight relationship between the predicted value and the observed value, is calculated as follows:

$$\boldsymbol{K}_{i+1} = \boldsymbol{C}^{xy}_{i+1|i}\left(\boldsymbol{C}^{yy}_{i+1|i} + \boldsymbol{R}_{i+1}\right)^{-1} \tag{9}$$

$$\boldsymbol{C}^{xy}_{i+1|i} = \frac{1}{N-1}\sum_{i=1}^{N}\left(\boldsymbol{x}_{i+1|i} - \overline{\boldsymbol{x}}_{i+1|i}\right)\left(\boldsymbol{y}_{i+1|i} - \overline{\boldsymbol{y}}_{i+1|i}\right)^T \tag{10}$$

$$\boldsymbol{C}^{yy}_{i+1|i} = \frac{1}{N-1}\sum_{i=1}^{N}\left(\boldsymbol{y}_{i+1|i} - \overline{\boldsymbol{y}}_{i+1|i}\right)\left(\boldsymbol{y}_{i+1|i} - \overline{\boldsymbol{y}}_{i+1|i}\right)^T \tag{11}$$

where, $\boldsymbol{C}^{xy}_{i+1|i}$ is the state variable prediction covariance matrix, $\boldsymbol{C}^{yy}_{i+1|i}$ is the predicted error covariance matrix of observed variables, $\overline{\boldsymbol{x}}_{i+1|i}$ is the ensemble mean of predict state variables, $\overline{\boldsymbol{y}}_{i+1|i}$ is the ensemble mean of predicted values of observed variables, and N is the number of ensembles.

In the current study, the extended state variable matrix $\boldsymbol{Z}=(\boldsymbol{\theta}, \boldsymbol{x})^T$ was established by updating the state variables and model parameters simultaneously. Where, $\boldsymbol{\theta}$ is the saturated hydraulic conductivity (K_s) of the filler layer; and x is the outflow rate (q) or surface water depth (h_p) of the grassed swale. According to the existing research and the actual situation in this study, the ensemble number of Ensemble Kalman filter was set as 500 (Franssen and Kinzelbach, 2009), and standard deviations of K_s of the two grassed swales were set to 0.001 (Enschede) and 0.01 (Utrecht) (by experience).

The standard deviation of the model state variable was set by the percentage method which was set as 5 % in this study (Deng et al., 2016). Prior to apply the EnKF method to the assimilation of K_s into current work, a pseudo experiment was carried out to validate the feasibility of using EnKF method to estimate the K_s in the hydrological model, and to compare the effect of different observation errors on K_s estimation results. In the validation process, the 'true value' of K_s was a given sequence, and these sequences were in 4 conditions (constant, periodic, periodic and incremental, and jumping) to simulate the possible trends of K_s (Deng et al., 2016). A sequence of K_s was put into the hydrological model, and a sequence of state variables (h_p, q) would be obtained. This sequence was used as the observation variable in EnKF, and the estimated values of K_s were calculated through EnKF, which were used to compare with the 'true value'. For example, at time t, the initial values of model parameters, state variables, and basic data such as rainfall were put into the hydrological model, the predicted values of state variables h_p and q at time t+1 could be obtained. Assumed the number of ensembles as 500, a Monte Carlo method was used to randomly generate state vector prediction ensembles and observation variable ensembles based on model error and observation error. Then, the Kalman gain factor was obtained by calculating the state variable prediction covariance matrix and the predicted error covariance matrix of observed variables. Thus, the analysis ensemble of model parameters and state variables at time t+1 could be obtained, with the mean of the ensemble as the final estimated value. Next, the estimated value of parameters and state variables were used as model inputs at the time t+1, and the above process were repeated until the end of rainfall. The variance levels of observation were set as 0, 5%, and 10% of the measure range, respectively.

2.4. Multivariate nonlinear model of K_s

Various parameters were analyzed for MvNR analysis, including influencing factors of K_s as x_1 (antecedent dry period/day), x_2 (temperature/°C), x_3 (rainfall/mm), x_4 (rainfall duration/h), x_5 (total rainfall/mm), and x_6 (seasonal factors). The functional relationship between K_s and each influencing factor can be expressed as $f_1(x_1)$, $f_2(x_2)$, $f_3(x_3)$, $f_4(x_4)$, $f_5(x_5)$ and $f_6(x_6)$, respectively. When considering six influencing factors simultaneously, it can be considered that K_s is the weighted sum of six factors, so K_s can be expressed as:

$$\begin{aligned}\mathbf{y} = \boldsymbol{c}_1\boldsymbol{f}_1(\boldsymbol{x}_1) + \boldsymbol{c}_2\boldsymbol{f}_2(\boldsymbol{x}_2) + \boldsymbol{c}_3\boldsymbol{f}_3(\boldsymbol{x}_3) + \boldsymbol{c}_4\boldsymbol{f}_4(\boldsymbol{x}_4) + \boldsymbol{c}_5\boldsymbol{f}_5(\boldsymbol{x}_5) \\ + \boldsymbol{c}_6\boldsymbol{f}_6(\boldsymbol{x}_6)\end{aligned} \tag{12}$$

The data used for MvNR and SCE-UA are listed in Tables S3 and S4, which included 95 rainfall events from Enschede swale and 58 rainfall events from Utrecht, and the K_s values were obtained by EnKF. A multiple nonlinear regression analysis was conducted that linear function, exponential function, power function, logarithmic function and quadratic polynomial function were selected to express the relationship between influencing factor and K_s. The influencing factors were the independent variable and K_s was the dependent variable and implemented by SPSS software. The fitting formulas corresponding to the six influencing factors were added to get the final function type.

The SCE-UA (Shiffled Complex Evolution-University of Arizona) algorithm (Duan et al., 1993), which is a global optimization algorithm commonly used in the field of hydrology, was used to calibrate the coefficient of each variable of the obtained K_s function. When a sequence of coefficients gets the minimum value of root mean square error (*RMSE*) between the calculated and real values (EnKF) of K_s for all rainfall events (objective function), it was considered as the optimal one. The calculation process of SCE-UA is presented in Fig. S1 (Duan et al., 1993). The final function of K_s was brought into the hydrological model for verification where 58-rainfall data of Utrecht swale were used. The simulation total relative error (*VE*) of the simulated outflow and peak flow were compared and analyzed between two conditions: K_s calculated by the function and K_s was constant. A sensitivity analysis of the final function was carried out to analyze the impact of each factor on K_s changes, and implemented by SimLab software.

2.5. Evaluating indicators

The Nash Sutcliffe efficiency coefficient (*NSE*) and the simulation total relative error (*VE*) were selected to evaluate the simulation and assimilation on the outflow and surface water depth of grassed swale.

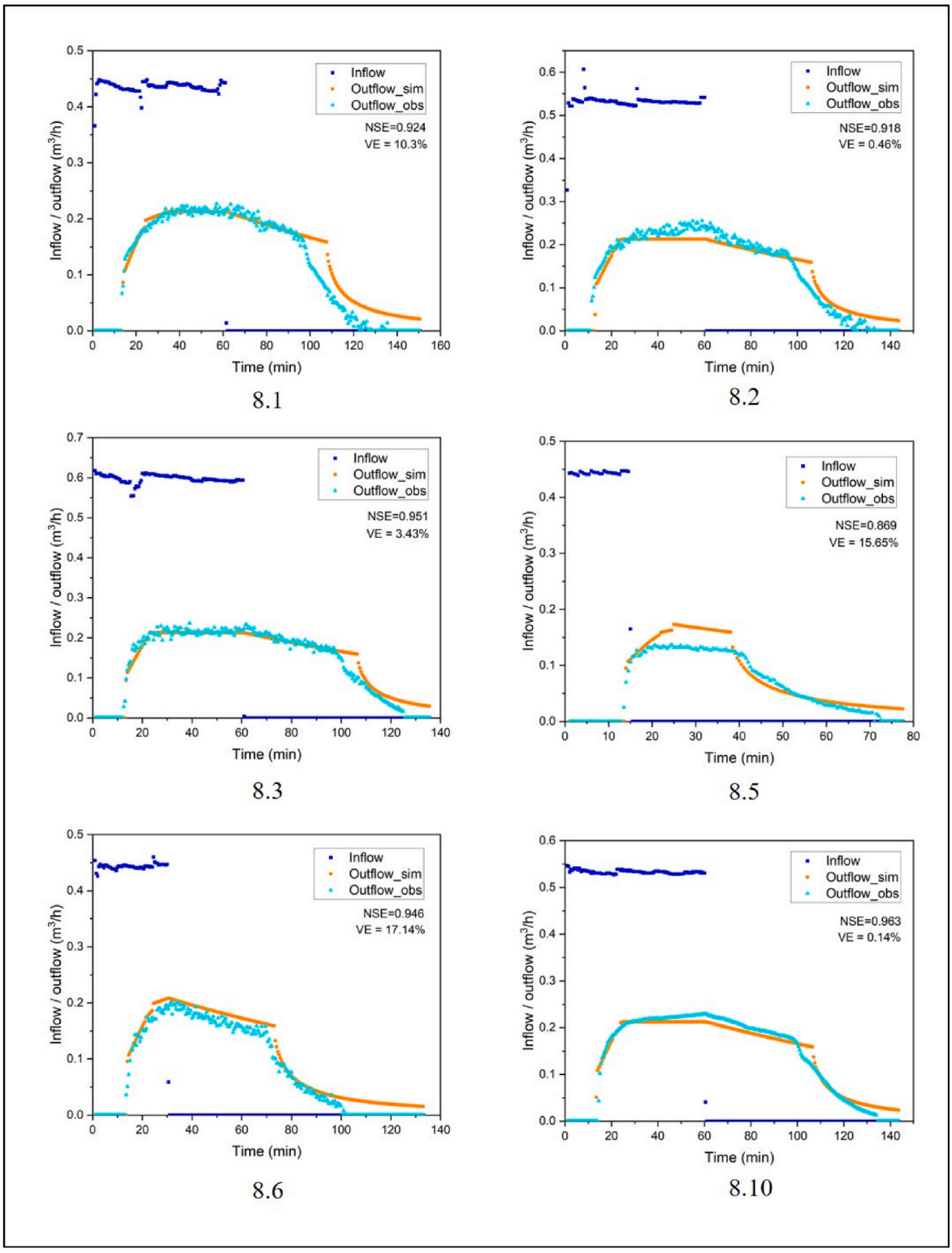

Fig. 1. Model simulation of outflow from grassed swale under different rainfall events.

$$NSE = 1 - \frac{\sum_{i=1}^{n}\left(x_{sim,i} - x_{obs,i}\right)^2}{\sum_{i=1}^{n}\left(x_{obs,i} - \bar{x}_{obs}\right)^2} \quad (13)$$

$$VE = \left|\frac{\sum_{i=1}^{n} x_{sim,i} - \sum_{i=1}^{n} x_{obs,i}}{\sum_{i=1}^{n} x_{obs,i}}\right| \quad (14)$$

where, $x_{sim,i}$ is the simulation value, $x_{obs,i}$ is the observation value, $\bar{x}_{obs}$ is the average value of observation and n is the sequence length.

The Pearson correlation coefficient (R), root mean square error ($RMSE$) and absolute mean relative error ($MARE$) were used to evaluate the estimation results of the parameters.

$$R = \frac{\sum_{i=1}^{n}\left(\theta_{sim,i} - \bar{\theta}_{sim}\right)\left(\theta_{obs,i} - \bar{\theta}_{obs}\right)}{\sqrt{\left(\theta_{sim,i} - \bar{\theta}_{sim}\right)^2\left(\theta_{obs,i} - \bar{\theta}_{obs}\right)^2}} \quad (15)$$

$$RMSE = \sqrt{\frac{1}{n}\left(\sum_{i=1}^{n}\left(\theta_{sim,i} - \theta_{obs,i}\right)^2\right)} \quad (16)$$

$$MARE = \frac{1}{n}\sum_{i=1}^{n}\frac{\left|\theta_{sim,i} - \theta_{obs,i}\right|}{\theta_{obs,i}} \quad (17)$$

where, $\theta_{sim,i}$ is the estimate value of parameter, $\theta_{obs,i}$ is the 'true value' of parameter, $\bar{\theta}_{sim}$ is the average estimate value of parameter and $\bar{\theta}_{obs}$ is the average 'true value' of parameter.

3. Results and discussion

3.1. Verification of hydrological model

The outflow simulation results are presented in Fig. 1. Excluding the rainfall event on August 5th, the *NSE* values were all above 0.9, indicating that the performance of model simulation on outflow of shorter rainfall duration was not as good as that of longer events. Nonetheless, the *NSE* values were all above 0.85. The *VE* values of the model simulation results range from 0.14% to 17.4%, with relatively large fluctuations. The results also reveal that *NSE* relates to the consistency between the simulated and measured trend of outflow, while *VE* relates to the total amount of error.

The simulation results of the surface water level and peak flow rates are presented in Table 1. Overflow time was used to estimate the model accuracy of the surface water level of the grassed swale. The *VE* (n = 1) value were less than 10% in the simulation of overflow time, while the results of peak flow rate ranged from 3%–26.3%. Above mentioned results reveal that the model does not perform well in simulating peak flow rate of a grassed swale.

In general, the simulation model of short-term rainfall is poor, possibly due to the sustained presence of an unsaturated state of the filler layer after a relatively short period of rainfall. The unsaturated flow is greatly affected by the initial water content, while a constant value of initial water content has been used in the verification process, this emphasizes the importance of initial water content in simulating the hydrological performance of grassed swale (Rujner et al., 2018a,b). They have used Mike SHE models to simulate the hydrological performance of a grass swale and found the similar results that the best fit (*NSE* > 0.8) was obtained for high inflows and wet antecedent moisture conditions. When the duration of rainfall increases, the simulation result improves, indicating that the model has a better simulation effect of the saturated infiltration process. The poor performance in simulating the peak flow rate may be caused by the changing characteristics of the saturated hydraulic conductivity, while in the verification process it is constant.

Table 1
Model simulation of surface water level and peak flow rates of grassed swale under different rainfall events.

Date	Overflow time (min)			Peak flow rate (m^3/h)		
	Simulation value	True value	*VE*	Simulation value	True value	*VE*
2021.8.1	35	35	0	0.213	0.227	6.2%
2021.8.2	25.5	24	6.3%	0.212	0.256	17.2%
2021.8.3	21.5	20	7.5%	0.213	0.237	10.1%
2021.8.5	–	–	–	0.173	0.137	26.3%
2021.8.6	–	–	–	0.208	0.202	3.0%
2021.8.10	25	23	8.7%	0.213	0.229	7.0%

3.2. K_s assimilation of EnKF

3.2.1. Validation of EnKF in K_s assimilation

(a) h_p as the observation variable (Enschede)

The results on comparison between the estimated values true values of K_s under different scenarios when the observation variable was h_p, are presented in Fig. 2. The statistical indicator results are presented in Table 2. As shown in Fig. 2, the estimated K_s values obtained through EnKF are in good agreement with the true values, reflecting the actual trend of the changes.

In the low variance scenario, the estimated values of K_s had a smaller *RMSE* and a higher *R* value, possibly because the assimilation results might be influenced by the magnitude of error uncertainty. It is fact that the K_s was constant, the trend of assimilation results was basically consistent, but the degree of deviation from the true follows the increase of variance. When K_s followed a periodic change or increasing in cycles, with the increase of variance, although it can still reflect a periodic or increasing trend, the degree of deviation from the true value was also increasing. There was a significant lag time between the estimated values and the true values. The reason might be that in EnKF, the updates of model state variables and parameters are closely related to the Kalman gain, and their updates depend on the observed values at the current time. While the measured observed variable values at the current time are closely related to the state variables at the current and previous times. Therefore, lag time is prone to occur when the parameters have periodic changes. When K_s increased by leaps, the estimation results under different variance conditions were better than those under periodic changes. Data presented in Table 2 revealed that the K_s with constant or jump changes have lower *RMSE* and *MARE* values, as well as higher *R* values, compared to those of incremental changes.

(b) q as the observation variable (Utrecht)

Assuming that the observation variable was q, the comparison between the estimated values and true values of K_s under different scenarios is shown in Fig. 3. The statistical indicator results are presented in Table 3.

Results revealed that when K_s was constant, with the increase of the variance, the degree of deviation between estimated value and true value increases, and the 95% confidence interval range also increased. When K_s followed a periodic change, the change in variance had little impact on the estimation results. In case of a gradual increase in K_s, the degree of deviation also increased, meanwhile, it was more significantly affected by changes in variance. Higher variance with larger range of 95% confidence interval. This may attribute to the special T-shaped structure of swale in Utrecht, and the same filer in both filler and drainage layer. The K_s of drainage layer was no longer enough to discharge the upper layer inflow in time when K_s increased to a certain

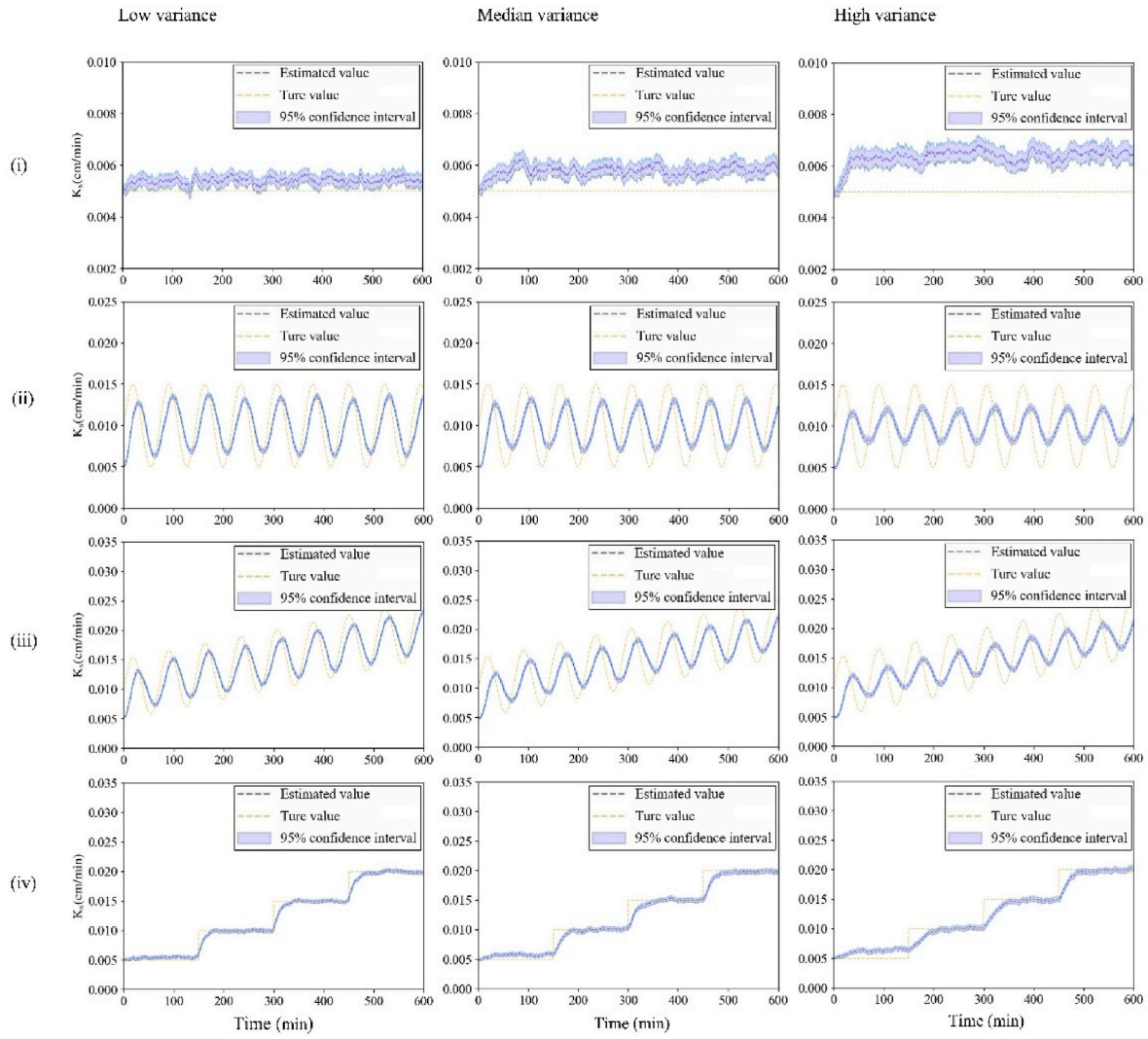

Fig. 2. K_s estimation results from Ensemble Kalman filter at different changing trend under three levels of variance with the observation variable h_p.

Table 2
Statistical indicator (RMSE, MARE, R) results between estimated and 'true' value of K_s under different level of observation variance(Observation variable is h_p).

Scenarios	Low variance			Median variance			High variance		
	RMSE	MARE	R	RMSE	MARE	R	RMSE	MARE	R
i	0.0004	0.0823	0	0.0008	0.1569	0	0.0014	0.2732	0
ii	0.0026	0.2518	0.6924	0.0035	0.3527	0.3339	0.0038	0.3908	0.0821
iii	0.0026	0.1667	0.822	0.0035	0.2247	0.6634	0.004	0.2532	0.5529
iv	0.0009	0.0496	0.9873	0.0011	0.0659	0.983	0.0014	0.1003	0.9736

value, and the control factor for the outflow rate becomes the K_s of the drainage layer. Table 3 also showed that compared to the incremental changes, K_s with constant or periodic changes had lower *RMSE* and *MARE* values, as well as higher *R* values. It is worth noting that the measured K_s value was less than 0.1 cm/m in 2020, which implied that it would not affect the assimilation results of EnKF.

Overall, good results have been obtained using the EnKF method coupled with the hydrological model to identify K_s of grassed swale filler layer by using outflow rate q or surface water depth h_p as observation variables.

3.2.2. *Applicability of EnKF into study sites*

Based on the results of the pseudo experiment, low variance error distribution was selected for the data analysis of the study sites.

(a) Enschede

Data assimilation results of K_s under partial rainfall events are presented in Fig. 4. It showed that the h_p estimated values by EnKF was in good agreement with the observation values, with *NSE* above 0.999 and *VE* below 0.002. In the initial stage (preheating stage), there was a significant fluctuation in the estimated value of K_s, which can be considered as a systematic error in the initial state. Fig. 4 also revealed that in the initial stage, the value h_p was basically 0. After this stage, the estimated value of K_s was close to a constant. This trend indicated that K_s remained largely unchanged during a single rainfall process, which is also consistent with the actual situation. At the end of the monitoring period, the K_s curve slightly increased. The possible reason could be that the surface of the real swale is irregular, while the model assumes a

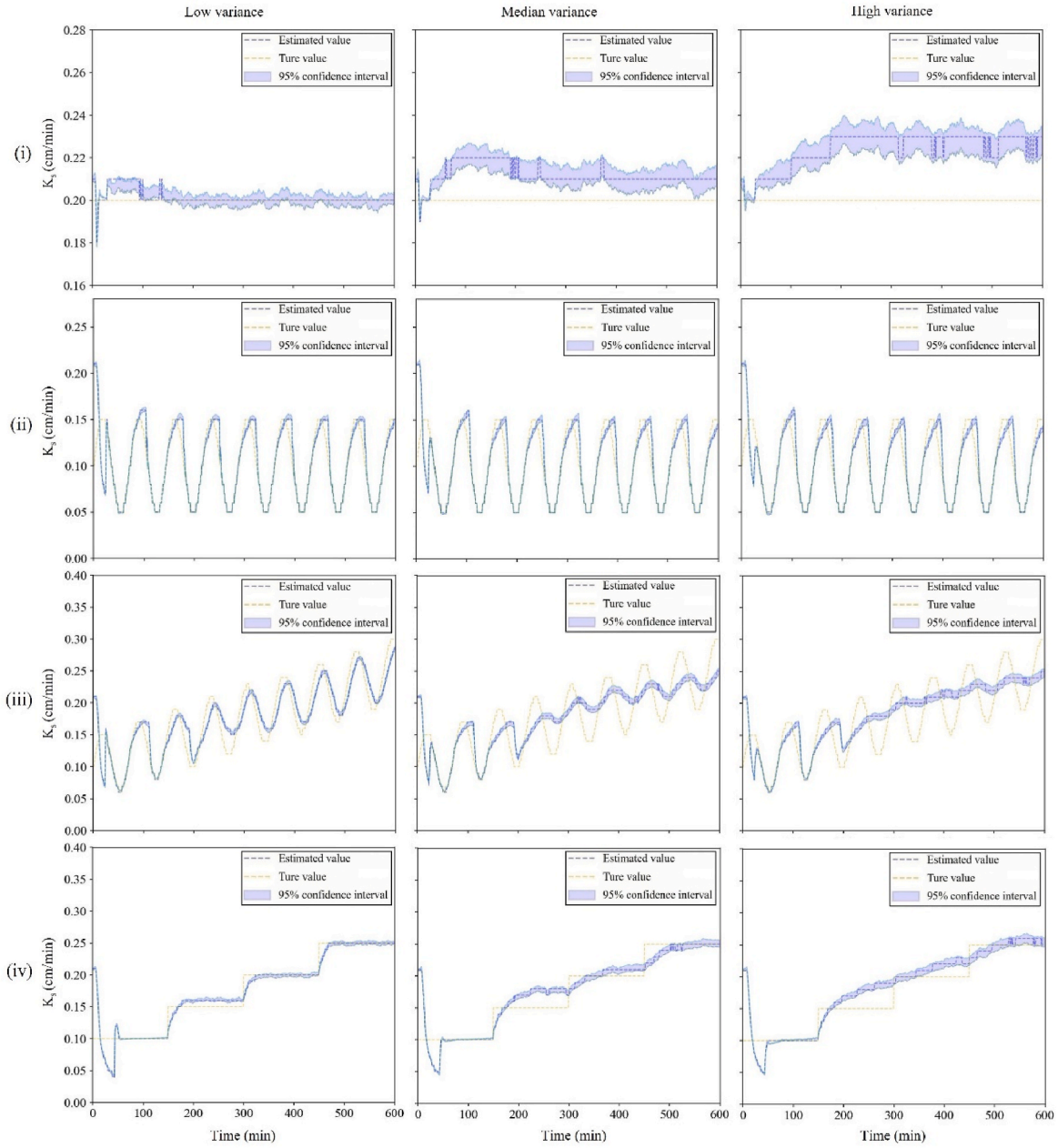

Fig. 3. K_s estimation results from the Ensemble Kalman filter at different changing trend under three levels of variance with the observation variable q.

Table 3
Statistical indicator (RMSE, MARE, R) results between estimated and 'true' value of K_s under different level of observation variance (Observation variable is q).

Scenarios	Low variance			Median variance			High variance		
	RMSE	MARE	R	RMSE	MARE	R	RMSE	MARE	R
i	0.004	0.007	0	0.014	0.066	0	0.027	0.128	0
ii	0.018	0.061	0.895	0.019	0.073	0.880	0.02	0.084	0.866
iii	0.024	0.109	0.9	0.033	0.158	0.798	0.035	0.171	0.789
iv	0.019	0.063	0.946	0.022	0.09	0.92	0.025	0.11	0.916

uniform surface. After the surface is emptied to a certain height while remaining some water in the low-lying areas, the entire layer becomes unsaturated and the decrease rate of h_p increases. This may explain the K_s increase at the end. Hence, an average value of the middle stage was taken as the estimated K_s of the filler layer in this grassed swale under a single rainfall.

Results of estimated K_s by EnKF (Fig. 5a) revealed a slightly decreasing trend year by year. Fig. 5b and c showed the seasonal characteristics of K_s for the whole data and the year of 2020–2021. Fig. 5b showed that K_s was significantly higher in summer than in other seasons, which may be caused by the evapotranspiration and plant growth in summer, while in 2020~2021 (Fig. 5c), the K_s in winter were significantly higher than those in other seasons. However, in summer, it showed a relatively lower value than other seasons, although there were

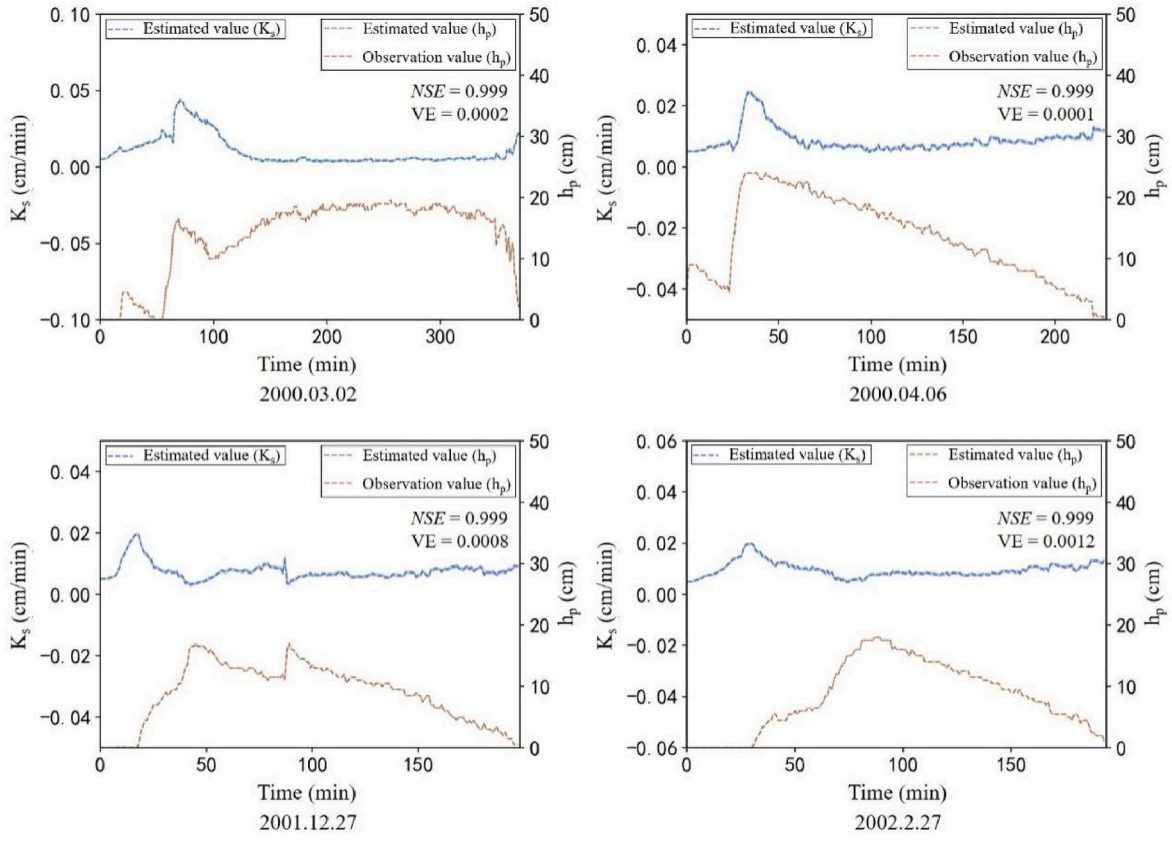

Fig. 4. K_s estimation results by the Ensemble Kalman filter under partial rainfall events (Enschede).

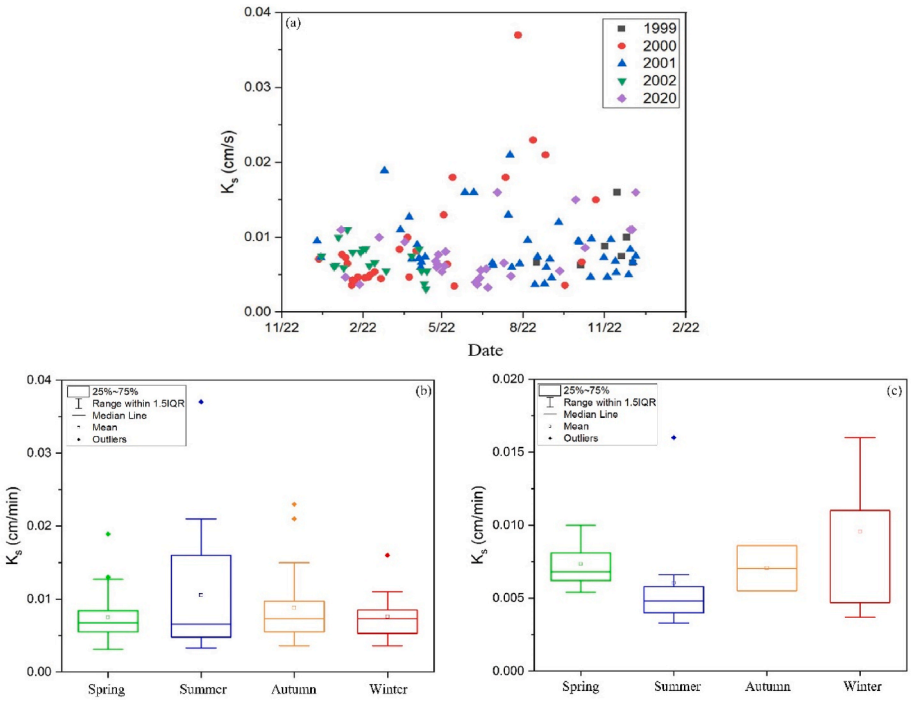

Fig. 5. Interannual and seasonal changing characteristics of K_s, (a, b) 1999–2021; (c) 2020–2021 (Enschede) (b) Utrecht.

some cases of high K_s values. When focused on the median value presented Fig. 5b, K_s in summer was slightly lower than other seasons while it was highest in winter. This trend was consistent with the values in 2020 and 2021. This revealed that the change characteristics of K_s at the beginning of construction are basically same as 20 years later. The difference was more outlier in the results of first three years, which might be caused by plant growth and instability of the whole system.

Results in summer revealed more dispersion proved that the

infiltration capacity of filler layer in the swale showed a partial recovery in summer. The strong evapotranspiration in summer may be the main reason for this phenomenon. Swale performance was stable after a prolonged operation and maintained a relatively low level of K_s in summer and did not reveal any significant recovery. This trend might be due the growth of grass roots, which mainly grew in the upper layer of fillers. The uncontrolled growth in summer caused their roots to intertwine on the surf. It is worth noting that in the winter of 2020, there was a heavy snowfall event in the Netherlands, the frequent snowfall and snowmelt processes have increased the soil moisture content, resulted into a frozen filler layer. As frost heave may induce restoration of the infiltration capacity (Zaqout and Andradóttir, 2021), this period of frost be an important reason for the significant increase in K_s values in the winter of 2020.

Data assimilation results of K_s under partial rainfall events are presented in Fig. 6. Results revealed that the q estimated by EnKF was in good agreement with the observation values, with *NSE* above 0.9 and *VE* less than 0.03. There was also a significant fluctuation of estimated K_s in the initial period which eliminates the system error in the beginning. The estimated q was consistent with the observations, while K_s remained unchanged. The estimated K_s curve showed a minor declining trend in the end. The filler was unsaturated in the empty period, when the swale started to be unsaturated but the model may still be in a saturated state, this may result in a small decrease in the estimating of K_s. As the results of case study of Enschede, only an average value of the middle stage was taken here as the estimated K_s of the filler layer of the grassed swale under a single rainfall.

The results of the estimated K_s by EnKF and its seasonal characteristic are presented in Fig. 7. Compared with the K_s value of 2009 (approximately 0.3 cm/min), there had been a significant decrease after ten-year's operation. The K_s values were higher in summer and winter in 2021, but lower in spring and autumn. Compared to the Enschede, results from the summer showed a different trend. Previous studies

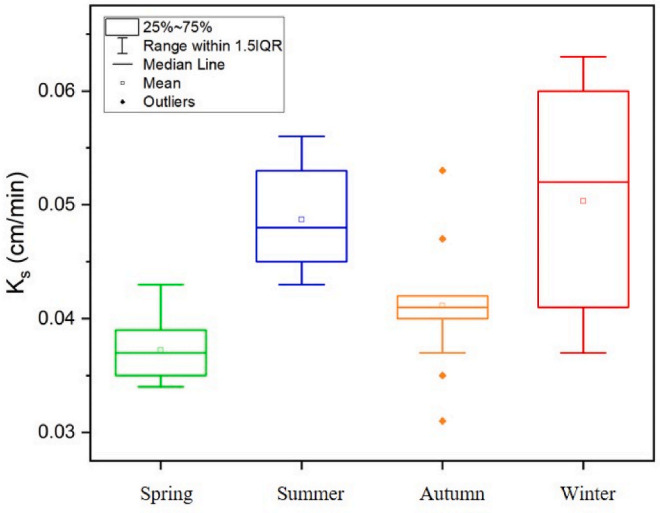

Fig. 7. Change in seasonal characteristics of K_s (2020–2021) (Utrecht).

revealed that the grass in the swale grown more luxuriantly in summer, meanwhile, its fillers had larger pores, which might enhance evapotranspiration (Li et al., 2017), and enlarged the pores and restored the infiltration capacity (Liu, 2020). Similar to the Enschede, there was an increasing trend in K_s in winter due to the heavy snow and the low temperature.

Findings from the Enschede/Utrecht case studies revealed that the K_s values of both grassed swales showed a significant decrease after long-term operation, but still maintain a notable hydrological performance. This trend was consistent with existing research findings focused on grassed swales and other related facilities (Coustumer et al., 2009; Haile

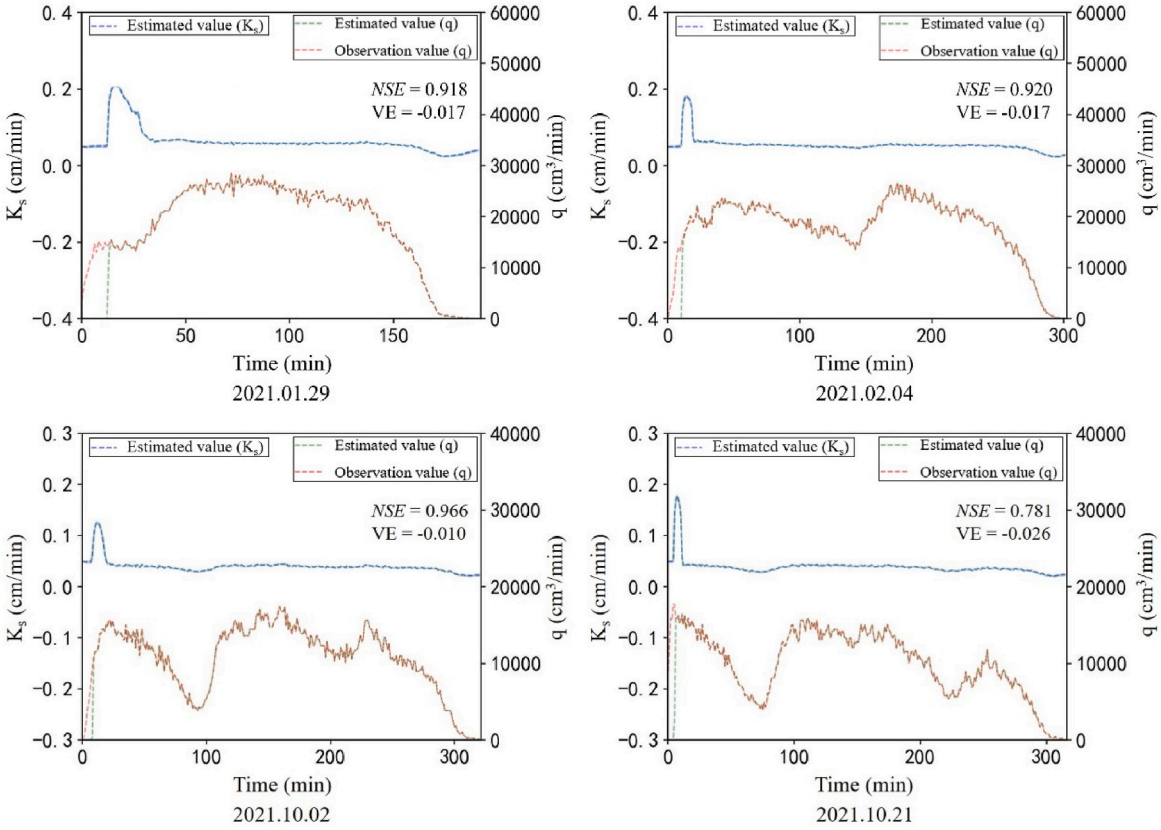

Fig. 6. K_s estimation results of the Ensemble Kalman filter under partial rainfall events (Utrecht).

et al., 2016; Willard et al., 2017). The lag between the K_s of two swales may result in the different soil composition (Coustumer et al., 2012). The type of vegetation, such as deep-rooted grass species and proliferation of root and earthworm channels, also improve infiltration (Dagenais et al., 2018; Fort et al., 2012; Muerdter et al., 2018). This might be related to the K_s recovery in summer and winter. Saudo-Fontaneda et al. (2020) conducted a long-term (3 years) hydrological monitoring research of a grass swale, and surface water level and temperature were recorded which consistent with current findings, but the method to evaluate the hydrological performance by comparison of surface water level seems not very precise somehow, while a combined model based on EnKF method can give more specific results. Grass swale resisted structural deformations resulting from frost, which was attributed to the high near-surface porosity within the intertwined root layer and the high drainage capacity of the underlying soil. Whereas, the non-vegetated site had 30 to 50 times lower infiltration during winter compared to the grass swale and twenty times lower during summer (Tarek et al., 2022). This indicates that vegetation plays an instrumental role in maintaining the hydrological functions of grassed swales both in winter and summer.

3.3. Multivariate nonlinear model of K_s

The relationship between K_s and influencing factors does not follow a uniform distribution, which may affect the effectiveness of non-linear fitting. While using all data for fitting. Therefore, as a comparison, using all data for fitting, segments of the original data based on the relationship between K_s and influencing factors in this study have been considered to calculate the median of data values within each segment for nonlinear regression fitting.

3.3.1. Models and parameter calibration

The results of nonlinear fitting are presented in Table S5. Data revealed that the quadratic function was optimal for fitting the relationship between K_s and each influencing factor in the Enschede swale from a comparison of the R^2 of the 5 listed curve types. While in Utrecht, in addition to the rainfall duration and seasonal factors, other factors were also following the quadratic function relationship. Although the R^2 value of the quadratic function was not the highest among the fitting results for these two influencing factors, the deviation from the optimal value was minimal. Hence, the quadratic function relationship was still considered valid. Therefore, the relationship between K_s and each influencing factor was expressed by quadratic function.

$$\mathbf{y} = C_1 x_1^{\,2} + C_2 x_1 + C_3 + C_4 x_2^{\,2} + C_5 x_2 + C_6 + C_7 x_3^{\,2} + C_8 x_3 + C_9 + C_{10} x_4^{\,2} + C_{11} x_4 + C_{12} + C_{13} x_5^{\,2} + C_{14} x_5 + C_{15} + C_{16} x_6^{\,2} + C_{17} x_6 + C_{18} \quad (18)$$

The SCE-UA algorithm was used to calibrate the parameter shown in Eq. (18). In this equation, $c_1 \sim c_{18}$ are the coefficients of each polynomial, the parameters that need to be calibrated. The results of the two swales are presented in Table 4.

The results of the parameter calibration (Table 4) revealed that the positive and negative characteristics of the quadratic and primary coefficients of the six influencing factors, except for temperature and seasonal factors, were consistent in the multivariate nonlinear models of each swale. This trend indicated that the difference of K_s between these two swales was mainly caused by temperature and seasonal changes. The differences of other coefficients, except for total rainfall, between the two swales were within one order of magnitude, which was caused by differences in the characteristic of the fillers. Both the initial saturated hydraulic conductivity and the monitoring results from 2021 showed a difference of one order of magnitude between the two swales. From the evaluation index of parameter calibration, the Enschede model had a higher *R* value and a lower *RMSE* value than the Utrecht model, as opposed to the *MARE* value. This indicated that the predicted results of the Enschede model were better than the Utrecht model in terms of correlation and statistical dispersion.

The validation results of hydrological model are shown in Table S6. And when K_s was time-varying from the multivariate nonlinear function, 37 events showed a decrease in the *VE* value of total outflow and peak flow compared to the model results when K_s was constant, with a proportion of 63.8%. When K_s was constant, the average value of *VE* was 29.2% and 24.5%, respectively; and When K_s was time-varying, the value decreased to 25.9% and 21.8% respectively. Therefore, in hydrological model, a time-varying K_s can improve the accuracy of model simulation.

3.3.2. Sensitivity analysis of multilinear model

The sensitivity analysis results are shown in Fig. 8 and, where (a) is the first-order sensitivity and (b) is the total-order sensitivity. The sensitivity of the six influencing factors of the Enschede model was as follows: rainfall > rainfall duration > temperature > antecedent dry period > total rainfall > seasonal factors, while in Utrecht, the sequence was seasonal factors > temperature > total rainfall > rainfall duration > antecedent dry period > rainfall. K_s values of the two swales showed great differences in temperature and seasonal factors. Firstly, the filler of the Enschede grassed swale uses improved soil, while Utrecht uses coarse sand. The porosity of the latter is significantly larger than the former, which is also the reason for the difference in initial K_s. Especially when the temperature was high in summer, the filler with large pores had a higher evaporation than that the one with small pores (Li et al., 2017), and evaporation could also increase the porosity of the fillers (Liu, 2020). Therefore, the K_s of the filler with the large pores exhibit an increase as temperature increases or in summer time. Secondly, the Enschede swale is planted with short turf, while the Utrecht swale is planted with relatively tall grass plants which grow vigorously in summer. Dense branches and leaves increase evapotranspiration, and growth of roots also helps to restore porosity. However, the relatively short grass vegetation has limited evapotranspiration. On the contrary, the rapid expansion of its fine roots on the surface may have a negative effect on the infiltration capacity of small porous fillers (Dagenais et al., 2018; Ebrahimian et al., 2019; Skorobogatov et al., 2020). The strong influence of summer plants may also be the reason why the fitting degree of the multivariate nonlinear model of the Utrecht grassed swales was

Table 4
The value of coefficients in the multivariate nonlinear function obtained by SCE-UA algorithm.

Coefficient	C_1	C_2	C_3	C_4	C_5	C_6	C_7	C_8	C_9
Enschede	−5.38 e^{-5}	5.57 e^{-4}	−8 e^{-4}	−2.23 e^{-6}	−3.67 e^{-5}	−2.64 e^{-3}	−7.93 e^{-6}	4.91 e^{-4}	3.04 e^{-3}
Utrecht	−7.53 e^{-4}	2.89 e^{-3}	5.98 e^{-2}	9.54 e^{-5}	−2.04 e^{-3}	1.36 e^{-2}	−6.82 e^{-6}	1.56 e^{-4}	1.31 e^{-2}
Coefficient	C_{10}	C_{11}	C_{12}	C_{13}	C_{14}	C_{15}	C_{16}	C_{17}	C_{18}
Enschede	7.15 e^{-6}	−3.41 e^{-4}	−1.19 e^{-3}	−3.12 e^{-11}	5.45 e^{-7}	5.93 e^{-3}	−3.21 e^{-5}	2.16 e^{-4}	−4.14 e^{-4}
Utrecht	2.47 e^{-5}	−7.9 e^{-4}	−3.56 e^{-2}	−1.73 e^{-8}	3.43 e^{-4}	−1.69	1.11 e^{-3}	−1.74 e^{-3}	−5.13 e^{-3}
Evaluating indicators				*R*		*RMSE*		*MARE*	
Enschede				0.734		0.0013		18.2%	
Utrecht				0.632		0.0061		11.1%	

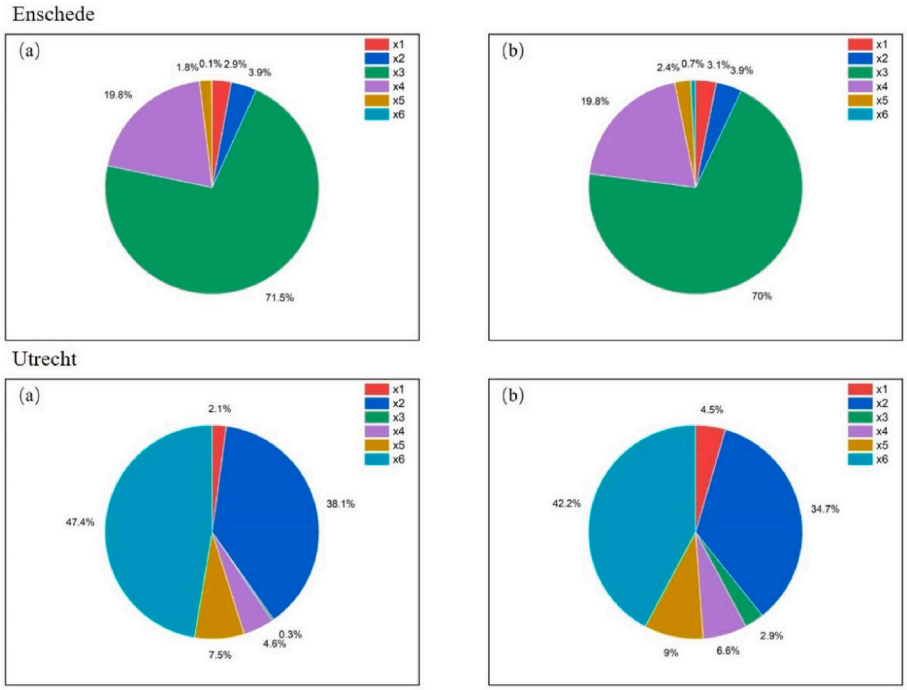

Fig. 8. Sensitivity analysis of multivariate nonlinear model of K_s: (a) First-order sensitivity, and (b) Total-order sensitivity.

not as good as the former, because seasonal factors may not fully reflect the effects of plant growth and evapotranspiration. In winter or regions with cold climates, the hydrological effects of most grassed swales or other facilities were suppressed because freezing of pore water hinders the infiltration process (Kratky et al., 2017).

However, other researchers pointed out that due to preferential flow, the saturated hydraulic conductivity of granular or porous media under frost conditions may be greater than that of unfrozen soil (Lefevre et al., 2009; Stoeckeler and Weitzman, 1960). This could explain the abnormal increase of K_s in the winter of 2020. A case study conducted by Ahmed et al. (2015) also emphasized the importance of plant in maintain the K_s, but also pointed out that the high spatial variation of K_s in the same swale and use a geometric mean K_s value. This may result in the non-relationship between seasonal index, filler type and K_s value. Therefore, it is important to test the K_s of the whole layer. In addition, human activity, maintenance and enrichment of pollutants would also influence the K_s of filler layer (Everett et al., 2023; Gyawali et al., 2021; Mohamed et al., 2014) need more data for verification. As the Utrecht grassed swale has only one year data, further study is required to determine whether it can accurately represent the long-term characteristics.

4. Field applications and future research prospective

4.1. Field applications

Previous study noted the high spatial variation of K_s in the similar swale and found that it is not easy to get the K_s of the whole filler layer (Ahmed et al., 2015). To better understand this issue, Boogaard (2022) investigated a saturated swale under artificial rainfall conditions and that K_s has strong relation with rate of surface water decrease. But, water resources and cost issues make it unable to become a long-term monitoring plan. Therefore, in this study, a hydrological model coupled with EnKF method was established and proved suitable for inverting the K_s of filler layer in grassed swales. The monitoring of surface water level and outflow rate under nature rainfall seems more automated and economical. The effluent flow meters could be installed in the swale outlets to monitor the effluent conditions. The monitoring priority should be given to the outflow rate, because it may not have a surface ponding during small rainfall events. However, in the field, it is not easy to install and operate the equipment and the surface water level become the best choice for data collection. In case of using surface water level as observed variable, the depth of drainage layer has no impact on model inversion results as K_s of drainage layer is large enough compared with filler layer. This can solve the aging issue of swales as their underground size and depths are not clear. This method can also be used for other infiltration facilities, such as bioretention, raingarden, etc. The multivariate nonlinear model of K_s can be used to modify the hydrological model and make the model prediction more accurate in the long-term simulation.

4.2. Future research prospective

The prospects for future research mainly include three points:

(i) Inclusion of long-term monitoring parameters

Although this work is a long-term study, the recorded data is still very limited on various parameters. Different types, fillers, vegetation cover, and different regions of grassed swales should be included in the long-term monitoring system at the same time scale. The monitoring factors include rainfall, temperature, surface water level or outflow rate under natural rainfall events. Swale's characteristics should also be recorded for better understanding. The method established in this study is used to find out the K_s value and obtain more general conclusions.

(ii) Quantifying the impact of plants, evaporation and other environment factors

The growth of plant roots and evaporation have been proven to have a positive effect on the restoration of infiltration capacity in grassed swales, but there is a lack of quantitative analysis in the existing research. The model of K_s may need to combine with the plant root growth model and evaporation model for the future research. Other factors such as anthropogenic activities or maintenance issues should be considered as well.

(iii) Selection of representative monitoring samples

It is unrealistic to conduct long-term monitoring of all grassed swales. Therefore, this requires statistical analysis of grassed swales with long-term monitoring data and identification of representative data sets. Representativeness here refers that the K_s model obtained through these data (multivariate nonlinear fitting) has similar predictive results to the model obtained through complete long-term data set, which will make the monitoring work more targeted and also save the manpower and material resources.

5. Conclusions

An approach for calculating the saturated hydraulic conductivity (K_s) of the filter layer in grassed swales using a hydrological model based on Ensemble Kalman filter algorithm was proposed in the current study. Two long-term operational grassed swales in the Netherlands have been selected in this study. The relationship between their K_s and influencing factors were also investigated. The pseudo experiment revealed a significant correlation between the observation variables (surface water level (h_p) and outflow (q)) and the estimated value of K_s. The K_s of the drainage layer would affect the estimation accuracy when it was not large enough compared to the filter layer. The error of EnKF estimation increased with an increase of the observation error. In the case study, the K_s values of both grassed swale's filler layer showed a significant decrease after long-term operation, but in summer and winter, K_s experienced a certain degree of recovery. The results of multiple nonlinear regression showed that the relationship between K_s and its influencing factors can be fitted by a quadratic function. After adding the Multivariate nonlinear function of K_s into the hydrological model, 63.8% of the predicted results were optimized among the validation events, which compared with a constant K_s. Results of sensitivity analysis showed that the degree of effect of each influencing factors on K_s varies depending on the type of grassed swale, fillers with lager pores and covered by thick grass or plants may be more sensitive to seasonal and temperature changes due to evapotranspiration in summer and frost swelling in winter.

CRediT authorship contribution statement

Feikai Yang: Conceptualization, Data curation, Formal analysis, Funding acquisition, Investigation, Methodology, Software, Validation, Writing – original draft, Writing – review & editing. **Dafang Fu:** Conceptualization, Data curation, Funding acquisition, Project administration, Resources, Supervision, Validation. **Chris Zevenbergen:** Conceptualization, Data curation, Methodology, Resources, Software, Supervision, Writing – review & editing. **Floris C. Boogaard:** Conceptualization, Data curation, Methodology, Project administration, Resources, Software, Validation. **Rajendra Prasad Singh:** Conceptualization, Data curation, Funding acquisition, Investigation, Methodology, Software, Supervision, Validation, Writing – original draft, Writing – review & editing.

Declaration of competing interest

The authors declare that they have no known competing financial interests or personal relationships that could have appeared to influence the work reported in this paper.

Data availability

Data will be made available on request.

Acknowledgement

This work was financially supported by the China Scholarship Council (CSC No. 201906090081) and Jiangsu Provincial Key R&D Programme (Social Development) (Grant No. BE2022820).

Appendix A. Supplementary data

Supplementary data to this article can be found online at https://doi.org/10.1016/j.jenvman.2023.119760.

References

Abualfaraj, N., Cataldo, J., Elborolosy, Y., Fagan, D., Woerdeman, S., Carson, T., et al., 2018. Monitoring and modeling the long-term rainfall-runoff response of the Jacob K. Javits center green roof. Water 10 (11), 1494.
Ahmed, F., Gulliver, J.S., Nieber, J.L., 2015. Field infiltration measurements in grassed roadside drainage ditches: spatial and temporal variability. J. Hydrol. 530 (1), 604–611.
Akter, S., 2021. Modified Ensemble Kalman filter for reservoir parameter and state estimation in the presence of model uncertainty. J. Pet. Sci. Eng. 199 (1), 108323.
Al-Rubaei, A.M., Viklander, M., Blecken, G.T., 2015. Long-term hydraulic performance of stormwater infiltration systems. Urban Water J. 12 (8), 660–671.
Amol, P., Raaj, R., 2018. Improved streamflow simulations by coupling soil moisture analytical relationship in EnKF based hydrological data assimilation framework. Adv. Water Resour. 121, 173–188.
Boogaard, F.C., 2022. Spatial and time variable long term infiltration rates of green infrastructure under extreme climate conditions, drought and highly intensive rainfall. Water 14 (6), 840.
Brown, R.A., Skaggs, R.W., Hunt, W.F., 2013. Calibration and validation of DRAINMOD to model bioretention hydrology. J. Hydrol. 486, 430–442.
Corner, S.P., 2022. The sixth major IPCC assessment report and its implications: 15 September 2021. Weather 77 (2), 70–71.
Coustumer, S.L., Fletcher, T.D., Deletic, A., Barraud, S., Poelsma, P., 2012. The influence of design parameters on clogging of stormwater biofilters: a large-scale column study. Water Res. 46 (20), 6743–6752.
Coustumer, S.L., Fletcher, T.D., Deletic, A., Barraud, S., Lewis, J.F., 2009. Hydraulic performance of biofilter systems for stormwater management: influences of design and operation. J. Hydrol. 376 (1–2), 16–23.
Dagenais, D., Brisson, J., Fletcher, T.D., 2018. The role of plants in bioretention systems; does the science underpin current guidance? Ecol. Eng. 120, 532–545.
Deletic, A., 2000. Sediment Behaviour in Overland Flow over Grassed Areas. University of Aberdeen.
Deng, C., Liu, P., Guo, S., Li, Z., Wang, D., 2016. Identification of hydrological model parameter variation using ensemble Kalman filter. Hydrol. Earth Syst. Sci. 20 (12), 4949–4961.
Donkers, B.E., 2010. Swale Filter Drain System: Inflow-Discharge Relation. Delft University of Technology.
Duan, Q.Y., Gupta, V.K., Sorooshian, S., 1993. Shuffled complex evolution approach for effective and efficient global minimization. J. Optim. Theor. Appl. 76 (3), 501–521.
Ebrahimian, A., Wadzuk, B., Traver, R., 2019. Evapotranspiration in green stormwater infrastructure systems. Sci. Total Environ. 688, 797–810.
Ellis, B., Lundy, L., Revitt, M., 2022. An Integrated Decision Support Approach to the Selection of Sustainable Urban Drainage Systems (SUDS). Switchtraining eu.
Everett, G., Matsler, A.M., Chan, F.K.S., Naclerio, M.A., Morzillo, A.T., Lamond, J.E., 2023. Lifestyle and language barriers influence community engagement with green infrastructure. Ambio 52, 1650–1660.
Fletcher, T.D., Shuster, W., Hunt, W.F., Ashley, R., Butler, D., Arthur, S., et al., 2015. SUDS, LID, BMPs, WSUD and more – the evolution and application of terminology surrounding urban drainage. Urban Water J. 12 (7), 525–542.
Fort, F., Jouany, C., Cruz, P., 2012. Root and leaf functional trait relations in Poaceae species: implications of differing resource-acquisition strategies. J. Plant Ecol. 6 (3), 211–219.
Franssen, H., Kinzelbach, W., 2009. Ensemble Kalman filtering versus sequential self-calibration for inverse modelling of dynamic groundwater flow systems. J. Hydrol. 365 (3–4), 261–274.
Fw, A., Ghha, B., Yf, C., Ypl, A., 2022. Development of a disaggregated multi-level factorial hydrologic data assimilation model. J. Hydrol. 610, 127802.
Geerling, H.R., 2014. Infiltration Swales: Quantitative Performance on an Urban Catchment Scale. Delft University of Technology.
Genuchten, V., Th, M., 1980. A closed-form equation for predicting the hydraulic conductivity of unsaturated soils. Soil Sci. Soc. Am. J. 44 (5), 892–898.
Girotto, M., Musselman, K.N., Essery, R.L.H., 2020. Data assimilation improves estimates of climate-sensitive seasonal snow. Curr. Clim. Change Rep. 6 (3), 81–94.
Gyawali, K., Babbar-Sebens, M., Radniecki, T.S., 2021. Dynamic treatment of county maintenance and service facility stormwater by a pump-fed bioswale system. J. Sustain. Water Built Environ. 7 (2), 04021003.
Haile, T.M., Hobiger, G., Kammerer, G., Allabashi, R., Schaerfinger, B., Fuerhacker, M., 2016. Hydraulic performance and pollutant concentration profile in a stormwater runoff filtration systems. Water Air Soil Pollut. 227 (1), 34.
Irvine, J.L., Kim, A.S., 2019. Hydraulic design perspectives of bioswale vegetation layers: a meta-research theory. Desalination Water Treat. 143, 137–147.
Jiang, Z., Huang, Q., Li, G., Li, G., 2019. Parameters estimation and prediction of water movement and solute transport in layered, variably saturated soils using the Ensemble Kalman Filter. Water 11 (7), 1520.

Kluge, B., Markert, A., Facklam, M., Sommer, H., Kaiser, M., Pallasch, M., et al., 2018. Metal accumulation and hydraulic performance of bioretention systems after long-term operation. J. Soils Sediments 18 (2), 431–441.
Kratky, H., Li, Z., Chen, Y., Wang, C., Li, X., Yu, T., 2017. A critical literature review of bioretention research for stormwater management in cold climate and future research recommendations. Front. Environ. Sci. Eng. 11 (4), 16.
Lefevre, N.J., Davidson, J.D., Oberts, G.L., 2009. Bioretention of simulated snowmelt: cold climate performance and design criteria. Cold Reg. Eng. 145–154.
Lou, W., Zhou, H.K., Yang, J.H., Hu, H., Sheng, L., 2022. Improving soil moisture estimation via assimilation of remote sensing product into the DSSAT crop model and its effect on agricultural drought monitoring. Rem. Sens. 14 (13), 3187.
Li, H.R., Chen, Y., Zhang, J.C., Xin, G.M., 2017. Evaporation in porous media with different porosity. CIE J. 68 (8) (in Chinese).
Liu, F.X., 2020. Study on Law and Effect of Soil Evaporation in Bare Soil under the Influence of Temperature and Humidity. Chang'an University (in Chinese).
Liu, Y., Engel, B.A., Flanagan, D.C., Gitau, M.W., McMillan, S.K., Chaubey, I., et al., 2018. Modeling framework for representing long-term effectiveness of best management practices in addressing hydrology and water quality problems: framework development and demonstration using a Bayesian method. J. Hydrol. 560, 530–545.
Mazrooei, A., Sankarasubramanian, A., 2019. Improving monthly streamflow forecasts through assimilation of observed streamflow for rainfall-dominated basins across the CONUS. J. Hydrol. 575, 704–715.
Mohamed, M.A.K., Lucke, T., Boogaard, F., 2014. Preliminary investigation into the pollution reduction performance of swales used in a stormwater treatment train. Water Sci. Technol. 69 (5), 1014–1020.
Muerdter, C.P., Wong, C.K., Lefevre, G.H., 2018. Emerging investigator series: the role of vegetation in bioretention for stormwater treatment in the built environment: pollutant removal, hydrologic function, and ancillary benefits. Environ. Sci. J. Integr. Environ. Res.: Water Res. Technol. 4 (5), 592–612.
Renato, Morbidelli, Carla, Saltalippi, Alessia, Flammini, et al., 2016. Laboratory investigation on the role of slope on infiltration over grassy soils. J. Hydrol. 543, 542–547.
Rossman, L.A., 2015. Storm Water Management Model User's Manual Version 5.1. U.S. EPA.
Rujner, Hendrik, Leonhardt, Gunther, Marsalek, Jiri, et al., 2018a. The effects of initial soil moisture conditions on swale flow hydrographs. Hydrol. Process. 32 (5), 644–654.
Rujner, H., Leonhardt, G., Marsalek, J., Viklander, M., 2018b. High-resolution modelling of the grass swale response to runoff inflows with Mike SHE. J. Hydrol. 562, 411–422.
Saracoglu, K.E., Kazezyilmaz-Alhan, C.M., 2023. Determination of grass swale hydrological performance with rainfall-watershed-swale experimental setup. J. Hydrol. Eng. 28 (3).
Saudo-Fontaneda, L.A., Roces-García, J., Coupe, S.J., Barrios-Crespo, E., Rey-Mahía, C., Lvarez-Rabanal, F.P., et al., 2020. Descriptive analysis of the performance of a vegetated swale through long-term hydrological monitoring: a case study from Coventry. UK. Water 12 (10), 2781.
Shafique, M., Kim, R., Kyung-Ho, K., 2018. Evaluating the capability of grass swale for the rainfall runoff reduction from an urban parking lot, Seoul, Korea. Int. J. Environ. Res. Publ. Health 15 (3), 537.
Skorobogatov, A., He, J., Chu, A., Valeo, C., van Duin, B., 2020. The impact of media, plants and their interactions on bioretention performance: a review. Sci. Total Environ. 715, 136918.
Stoeckeler, J.H., Weitzman, S., 1960. Infiltration rates in frozen soils in northern Minnesota. Soil Sci. Soc. Am. J. 24 (2), 1188–1200.
Su, J., Lu, H., Zhu, Y., Cui, Y., Wang, X., 2019. Evaluating the hydrological utility of latest IMERG products over the upper Huaihe river basin, China. Atmos. Res. 225 (9), 17–29.
Tarek, Z., Hrund, Ó.A., Ólafur, A., 2022. Infiltration capacity in urban areas undergoing frequent snow and freeze–thaw cycles: implications on sustainable urban drainage systems. J. Hydrol. 607, 127495.
Wang, S., Ancell, B., Huang, C., et al., 2018. Improving robustness of hydrologic ensemble predictions through probabilistic pre- and post-processing in sequential data assimilation. Water Resour. Res. 54 (3), 2129–2151.
Wei, Q., Liu, J., Hong, Y., Sweetapple, C., 2018. An ensemble-based dynamic Bayesian averaging approach for discharge simulations using multiple global precipitation products and hydrological models. J. Hydrol. 558, 405–420.
Willard, L., Wynn-Thompson, T., Krometis, L., Neher, T., Badgley, B., 2017. Does it pay to be mature? Evaluation of bioretention cell performance seven years postconstruction. J. Environ. Eng. 143 (9), 04017041.
Wu, Q., Zuo, Q., Han, C., Ma, J., 2022. Integrated assessment of variation characteristics and driving forces in precipitation and temperature under climate change: a case study of Upper Yellow River basin, China. Atmos. Res. 272, 106156.
Xiufeng, S., Hua, Q., Wentao, L.U., 2019. Evolution of water sensitive urban design in Australia and its enlightenment to sponge city. Chinese Landscape Arch 35 (9), 67–71.
Young, B.N., Hathaway, J.M., Lisenbee, W.A., He, Q., 2018. Assessing the runoff reduction potential of highway swales and WinSLAMM as a predictive tool. Sustainability 10 (8).
Yousef, Y.A., Hvitved-Jacobsen, T., Wanielista, M.P., Harper, H.H., 1987. Removal of contaminants in highway runoff flowing through swales. Sci. Total Environ. 59, 391–399.
Zaqout, T., Andradóttir, H., 2021. Hydrologic performance of grass swales in cold maritime climates: impacts of frost, rain-on-snow and snow cover on flow and volume reduction. J. Hydrol. 597 (11), 126159.